FRII*CAT*: A FIRST catalog of FR II radio galaxies.

A. Capetti[1], F. Massaro[2], and R.D. Baldi[3]

[1] INAF-Osservatorio Astrofisico di Torino, via Osservatorio 20, 10025 Pino Torinese, Italy,
[2] Dipartimento di Fisica, Università degli Studi di Torino, via Pietro Giuria 1, 10125 Torino, Italy,
[3] Department of Physics and Astronomy, University of Southampton, Highfield, SO17 1BJ, UK

ABSTRACT

We built a catalog of 122 FR II radio galaxies, called FRII*CAT*, selected from a published sample obtained by combining observations from the NVSS, FIRST, and SDSS surveys. The catalog includes sources with redshift ≤ 0.15, an edge-brightened radio morphology, and those with at least one of the emission peaks located at radius r larger than 30 kpc from the center of the host.
The radio luminosity at 1.4 GHz of the FRII*CAT* sources covers the range $L_{1.4} \sim 10^{39.5} - 10^{42.5}$ erg s^{-1}. The FRII*CAT* catalog has 90% of low and 10% of high excitation galaxies (LEGs and HEGs), respectively. The properties of these two classes are significantly different. The FRII*CAT* LEGs are mostly luminous ($-20 \gtrsim M_r \gtrsim -24$), red early-type galaxies with black hole masses in the range $10^8 \lesssim M_{\rm BH} \lesssim 10^9 M_\odot$; they are essentially indistinguishable from the FR Is belonging to the FR*CAT*. The HEG FR IIs are associated with optically bluer and mid-IR redder hosts than the LEG FR IIs and to galaxies and black holes that are smaller, on average, by a factor $\sim$2.
FR IIs have a factor $\sim$ 3 higher average radio luminosity than FR Is. Nonetheless, most ($\sim$ 90 %) of the selected FR IIs have a radio power that is lower, by as much as a factor of $\sim$100, than the transition value between FR Is and FR IIs found in the 3C sample. The correspondence between the morphological classification of FR I and FR II and the separation in radio power disappears when including sources selected at low radio flux thresholds, which is in line with previous results. In conclusion, a radio source produced by a low power jet can be edge brightened or edge darkened, and the outcome is not related to differences in the optical properties of the host galaxy.

Key words. galaxies: active – galaxies: jets

1. Introduction

Fanaroff & Riley (1974) introduced the first classification scheme for extragalactic radio sources with large-scale structures (i.e., greater than ~15-20 kpc in size) based on the ratio R_{FR} of the distance between the regions of highest surface brightness on opposite sides of the central host galaxy to the total extent of the source up to the lowest brightness contour in the radio images. Radio sources with R_{FR} <0.5 were placed in Class I (i.e., the edge-darkened FR Is) and sources with R_{FR} >0.5 in Class II (i.e., the edge-brightened FR IIs). This morphology-based classification scheme was found to be linked to their intrinsic power; Fanaroff and Riley found that all sources in their sample with luminosity at 178 MHz smaller than 2×10^{25} W Hz^{-1} sr^{-1} (for a Hubble constant of 50 km s^{-1} Mpc^{-1}) were classified as FR I while the brighter sources all were FR II. The luminosity distinction between FR classes is fairly sharp at 178 MHz; their separation is even cleaner in an optical-radio luminosity plane, implying that the FR I/FR II dichotomy depends on both optical and radio luminosity (Ledlow & Owen 1996).

The two Fanaroff-Riley classes do not instead correspond to a division from the point of view of the optical spectroscopic properties of their hosts. Laing et al. (1994) defined low and high excitation galaxies (LEGs and HEGs) based on the ratios of the diagnostic optical emission lines in a scheme similar to that adopted to distinguish LINERs and Seyferts in radio quiet AGN (Kewley et al. 2006). While all FR Is for which a reliable classification can be obtained are LEGs, both LEGs and HEGs are found among the FR IIs (e.g., Buttiglione et al. 2010). Buttiglione et al. find that LEGs and HEGs also differ from other points of view. While LEGs do not show prominent broad lines, they are observed in $\sim$ 30% of HEGs; narrow emission lines are a factor $\sim$ 10 brighter in HEGs than in LEGs at the same radio luminosity. Also, HEGs show bluer colors than LEGs (Smolčić 2009). Baldi & Capetti (2008) identify compact knots in the UV images of 3C HEG radio galaxies, a morphological evidence of recent star formation extending over 5−20 kpc; conversely, LEGs hosts are usually red, passive galaxies. These results suggest that the radio galaxies belonging to the two spectroscopic classes correspond to different manifestation of the radio loud AGN phenomenon (Hardcastle et al. 2007; Buttiglione et al. 2010; Best & Heckman 2012).

The recent multiwavelength large-area surveys are a unique tool to further explore the connection between the morphological and spectroscopic classes of radio galaxies, providing us with large samples of radio emitting AGN extending to lower luminosities than in previous studies.

In Capetti et al. (2017) we created a catalog of 219 edge-darkened FR I radio galaxies called FR*CAT*. We found that the FR*CAT* hosts are remarkably homogeneous, as they are all luminous red early-type galaxies (ETGs) with large black hole masses and spectroscopically classified as LEGs. All these properties are shared by the hosts of more powerful FR Is in the 3C sample. They do not show significant differences from the point of view of their colors with respect to the general population of massive ETGs. The presence of an active nucleus (and its level of activity) does not appear to affect the hosts of FR Is.

We now extend this study to the population of edge-brightened FR II radio galaxies with the main aim of comparing the properties of FR Is and FR IIs by also considering their spectroscopic classification.

This paper is organized as follows. In Sect. 2 we present the selection criteria of the sample of FR IIs. The radio and optical properties of the selected sources are presented in Sect. 3. Sect. 4 is devoted to results and conclusions.

Throughout the paper we adopt the same cosmology parameters used in Capetti et al. (2017), i.e., $H_0 = 67.8\,\mathrm{km\,s^{-1}\,Mpc^{-1}}$, $\Omega_\mathrm{M} = 0.308$, and $\Omega_\Lambda = 0.692$ (Planck Collaboration et al. 2016).

For our numerical results, we use c.g.s. units unless stated otherwise. Spectral indices α are defined in the usual convention on the flux density, $S_\nu \propto \nu^{-\alpha}$. The SDSS magnitudes are in the AB system and are corrected for the Galactic extinction; *WISE* magnitudes are instead in the Vega system and are not corrected for extinction since, as shown by, for example, D'Abrusco et al. (2014), such correction affects mostly the magnitude at 3.4 μm of sources lying at low Galactic latitudes (and by less than ∼3%).

2. Sample selection

We searched for FR II radio galaxies in the sample of 18,286 radio sources built by Best & Heckman (2012; hereafter the BH12 sample) by limiting our search to the subsample of objects in which, according to these authors, the radio emission is produced by an active nucleus. They cross-matched the optical spectroscopic catalogs produced by the group from the Max Planck Institute for Astrophysics and Johns Hopkins University (Brinchmann et al. 2004; Tremonti et al. 2004) based on data from the data release 7 of the Sloan Digital Sky Survey (DR7/SDSS; Abazajian et al. 2009),[1] with the National Radio Astronomy Observatory Very Large Array Sky Survey (NVSS; Condon et al. 1998) and the Faint Images of the Radio Sky at Twenty centimeters survey (FIRST; Becker et al. 1995; Helfand et al. 2015) adopting a radio flux density limit of 5 mJy in the NVSS. We focused on the sources with redshift $z < 0.15$.

We adopted a purely morphological classification based on the radio structure shown by the FIRST images. We visually inspected the FIRST images of each source and preserved those with an edge brightened morphology in which at least one of the emission peaks lies at a distance of at least 30 kpc from the center of the optical host. The 30 kpc radius corresponds to 11.″4 for the farthest objects; the $z < 0.15$ redshift limit ensures that all the selected sources are well resolved with the 5″ resolution of the FIRST images. The three authors performed this analysis independently and we included only the sources for which a FR II classification is proposed by at least two of us. We allowed for the presence of diffuse emission leading to X-, Z-, or C-shaped morphologies, but not extending at larger distances with respect to the emission peaks, thus excluding wide angle tail sources (Owen & Rudnick 1976). Most of these sources are double, i.e., they do not show nuclear radio emission; the lack of this precise position reference requires a further check of the original optical identifications. We discarded three objects in which the identification of the host is not secure.

The resulting sample, to which we refer as FRII*CAT*, is formed by 122 FR IIs whose FIRST images are presented in the Appendix. Their main properties are presented in Table 1, where we report the SDSS name, redshift, and NVSS 1.4 GHz flux density (from BH12). The [O III] line flux, the r-band SDSS AB magnitude, m_r, the Dn(4000) index (see Section 3 for its definition), and the stellar velocity dispersion σ_* are instead from the MPA-JHU DR7 release of spectrum measurements. The concentration index C_r was obtained for each source directly from the SDSS database. For sake of clarity, uncertainties are not shown in the table; we estimated a median uncertainty of 0.09 on C_r, of 0.03 on Dn(4000), of 0.005 magnitudes on m_r, and of 10 $\mathrm{km\,s^{-1}}$ on σ_*. We also list the resulting radio and line luminosity and the black hole masses estimated from the stellar velocity dispersion and the relation $\sigma_* - M_\mathrm{BH}$ of Tremaine et al. (2002). The uncertainty in the M_BH value is dominated by the spread of the relation used (rather than by the errors in the measurements of σ_*) resulting in an uncertainty of a factor ∼ 2. Finally, we give the classification (from BH12) into LEGs and HEGs based on the optical emission line ratios in their SDSS spectra.

[1] Available at `http://www.mpa-garching.mpg.de/SDSS/`.

3. FRII*CAT* hosts and radio properties

3.1. Hosts properties

The majority (107) of the selected FR IIs are classified as LEG, but there are also 14 HEG and just one source that cannot be classified spectroscopically because of the lack of emission lines, namely J1446+2142.

The distribution of absolute magnitude of the FRII*CAT* hosts covers the range $-20 \gtrsim M_r \gtrsim -24$ (see Fig. 1, left panel). The distribution of black hole masses (Fig. 1, right panel) is rather broad. Most sources have $8.0 \lesssim \log M_\mathrm{BH} \lesssim 9.0 M_\odot$, but a tail toward smaller values, down to $M_\mathrm{BH} \sim 10^{6.5} M_\odot$, that includes ∼ 15% (13 LEGs and 4 HEGs) of the sample.

The FR II HEGs are less luminous, overall, and harbor less massive black holes with respect to the FR II LEGs; the medians of their distributions are $< M_r(\mathrm{HEG}) >= -21.97 \pm 0.17$, $< M_r(\mathrm{LEG}) >= -22.62 \pm 0.06$, $< \log M_\mathrm{BH}(\mathrm{HEG}) >= 8.21 \pm 0.11$, and $< \log M_\mathrm{BH}(LEG) >= 8.46 \pm 0.04$, respectively. The comparison between the FRII*CAT* LEG sources and the FRI*CAT* hosts ($< M_r(\mathrm{FR\ I}) >= -22.69 \pm 0.03$ and $< \log M_\mathrm{BH}(\mathrm{FR\ I}) >= 8.55 \pm 0.02$) indicates that only marginal differences (and not statistically significant) are present between the medians of these distributions.

The Dn(4000) spectroscopic index, defined according to Balogh et al. (1999) as the ratio between the flux density measured on the red side and blue side of the Ca II break, is an indicator of the presence of young stars or of nonstellar emission. Low redshift ($z < 0.1$) red galaxies have Dn(4000)= 1.98 ± 0.05, which is a value that decreases to = 1.95 ± 0.05 for $0.1 < z < 0.15$ galaxies (Capetti & Raiteri 2015).

The concentration index C_r, which is defined as the ratio of the radii including 90% and 50% of the light in the r band, can be used for a morphological classification of galaxies, in which early-type galaxies have higher values of C_r than late-type galaxies. Two thresholds have been suggested to define ETGs: a more conservative value at $C_r \gtrsim 2.86$ (Nakamura et al. 2003; Shen et al. 2003) and a more relaxed selection at $C_r \gtrsim 2.6$ (Strateva et al. 2001; Kauffmann et al. 2003; Bell et al. 2003). Bernardi et al. (2010) found that the second threshold of the concentration index corresponds to a mix of E+S0+Sa types, while the first mainly selects ellipticals galaxies, removing the majority of Sas, but also some Es and S0s.

In Fig. 2 we show the concentration index C_r versus the Dn(4000) index (left panel) for the FRII*CAT* sources. More than ∼90% of the LEG FR II hosts lie in the region of high C_r and Dn(4000) values, indicating that they are red ETGs. The HEG FR II are still ETGs, but they show generally lower values of Dn(4000).

We also consider the $u-r$ color of the galaxies, obtained from SDSS imaging and thus referred to the whole galaxy rather than just the 3″ circular region covered by the SDSS spectroscopic

aperture. In Fig. 2 (central panel) we show the $u-r$ color versus the absolute r-band magnitude M_r of the hosts. As already found by considering the Dn(4000) index, the FR II HEGs show bluer color than the FR II LEGs; in this latter class, only two sources have a $u-r$ color that is smaller than the threshold separating red and blue ETGs (Schawinski et al. 2009).

In Fig. 2, right panel, we show the comparison of the *WISE* mid-IR colors of FRII*CAT* and FRI*CAT* sources; the associations with the *WISE* catalog are computed by adopting a 3.″3 search radius (D'Abrusco et al. 2013). All but one of the (J1121+5344) FRII*CAT* sources have a *WISE* counterpart, but 25 of these sources are undetected in the $W3$ band. The LEG FR IIs have mid-IR colors similar to those of the FRI*CAT* sources; their mid-IR emission is dominated by their host galaxies since they fall in the same region of elliptical galaxies (Wright et al. 2010). Only five LEGs have $W2-W3>2.5$, exceeding the highest value measured for FR Is.

Conversely, HEGs reach mid-IR colors as high as $W2-W3$=4.3, colors similar to those of Seyfert and starburst galaxies (e.g., Stern et al. 2005). Their red colors are likely due to a combination of star-forming regions and/or emission from hot dust within a circumnuclear dusty torus.

Overall, we found 10 LEG FR IIs whose properties do not conform with the general behavior of their class, for example, showing blue colors or being associated with small black holes. In some cases, this is due to relatively large errors particularly in the measurement of σ_*, a possible uncertain identification of their spectroscopic class, or a substantial contribution from a bright nonthermal nucleus. However, there are three objects (namely J0755+5204, J1158+3006, and J1226+2538) for which we obtain estimates of the black hole mass of $\log M_{\rm BH}\sim 6.5-6.8$; based on their C_r value these objects are late-type galaxies and two of them also show blue optical colors (and red mid-IR colors). These properties are all typical of radio quiet AGN. This contrasts with the observed radio power ($\log \nu L_r \sim 40.5-40.9$) and morphology.

3.2. Radio properties

The radio luminosity at 1.4 GHz of the FRII*CAT* covers the range $L_{1.4}=\nu_{\rm r} l_{\rm r}\sim 10^{39.5}-10^{42.5}$ erg s^{-1} (Fig. 3, left panel), reaching a radio power almost two orders of magnitude lower than the FR IIs in the 3C sample. The HEGs are brighter than LEGs (with median of $\log L_{1.4}=41.37$ and 40.76, respectively) and LEGs are brighter than the FRI*CAT* sources by a factor ∼3; 90% of the FRII*CAT* fall below the separation between FR Is and FR IIs originally reported by Fanaroff & Riley (1974) which translates, with our adopted cosmology and by assuming a spectral index of 0.7 between 178 MHz and 1.4 GHz, into $L_{1.4}\sim 10^{41.6}$ erg s^{-1}. Similarly, we find that ∼75% of the FRII*CAT* sources (and including also four HEGs) are located *below* the dividing line in the optical-radio luminosity plane defined by Ledlow & Owen (1996);[2] see Fig. 3, right panel.

FR IIs show a large spread in both radio and [O III] line luminosities (see Fig. 4). In this plane, the FR II LEGs cover essentially the same region of the FR Is with just a tail toward higher power both in line and in radio; no correlation is seen between these two quantities. The FR II HEGs generally have higher ratios between $L_{\rm [O\ III]}$ and $L_{1.4}$ than LEGs, which is an effect already found in the 3C sample (Buttiglione et al. 2010). The HEGs in FRII*CAT* are mostly located above the correlation defined by the 3C HEGs. A linear fit including both samples is indeed shallower (with a slope of 0.91) than that obtained from the 3C sources alone (whose slope is 1.15).

3.3. Comparison with previous works

As discussed in Sect. 2, we decided to maintain the traditional morphological visual classification into edge-brightened FR IIs and edge-darkened FR Is rather than adopting quantitative methods such as those used by Lin et al. (2010). The comparison of our classification with that proposed by these authors indicates that, among the 96 sources in common, ∼ 80% of the FRII*CAT* sources are classified as class *a* in their nomenclature, i.e., sources with two hot spots on either side of the galaxy. Most of the remaining objects fall in class *b*, in which the emission peak is coincident with the host galaxy; however, the inspection of these FR II radio sources does not show any clear distinguishing feature from those in the main class, other than having a relatively brighter central source in addition to the two lobes.

The main drawback of our scheme, based on the subjective visual inspection of radio images, is the relatively high fraction of sources of uncertain classification. The rather strict criteria adopted for a positive classification as FR I in Capetti et al. (2017) and here for the FR II enabled us to select only 219 FR Is and 122 FR II; more than half of the 714 radio galaxies extended more than 30 kpc cannot be allocated to any FR class. On the other hand, this strategy allows us to select samples that are very uniform from a morphological point of view and that are optimally suited for our main purpose, i.e., the comparison of the properties of the two classes.

More recently, Miraghaei & Best (2017) performed an analysis on the same initial sample, with an apparently similar selection strategy based on visual inspection. However, the resulting sample of both FR I and FR II differ significantly from those we obtained with only ∼ 25% of objects in common for both classes, even restricting the comparison to the same range of redshift, $0.03<z<0.15$. This mismatch is likely due to the different requirements (based, e.g., on linear instead of angular sizes and different radio flux limits); most importantly they considered only sources corresponding to multicomponents objects in FIRST and this rejects most of the edge darkened sources we included in FRI*CAT*. Overall, their results do not strongly differ from ours, probably because (leaving aside the HEGs) the properties of low z radio AGN are very homogeneous regardless of their radio morphology. However, for example, we do not find significative differences in the C_r values between FRI and FRII hosts.

4. Discussion and conclusions

The properties of the FRII*CAT* sources differ between those spectroscopically identified as LEGs or HEGs. The HEGs have lower optical luminosities, smaller black hole masses, and higher radio luminosities with respect to LEGs, although a substantial overlap between the two classes exist for all these quantities. The clearest differences are related to the ratio between line and radio luminosities and to their colors; HEGs are bluer in the optical and redder in the mid-IR. These results confirm the conclusions of previous studies (e.g., Baldi & Capetti 2008; Buttiglione et al. 2010; Baldi & Capetti 2010; Best & Heckman 2012).

The population of the LEG FR IIs included in the FRII*CAT* is remarkably uniform. They are all luminous red ETGs with

[2] We shifted the dividing line to the right of the diagram to include a correction of 0.12 mag to scale our total host magnitude to the $M_{24.5}$ used by these authors, and an additional 0.22 mag to convert the Cousin system into the SDSS system (Fukugita et al. 1996).

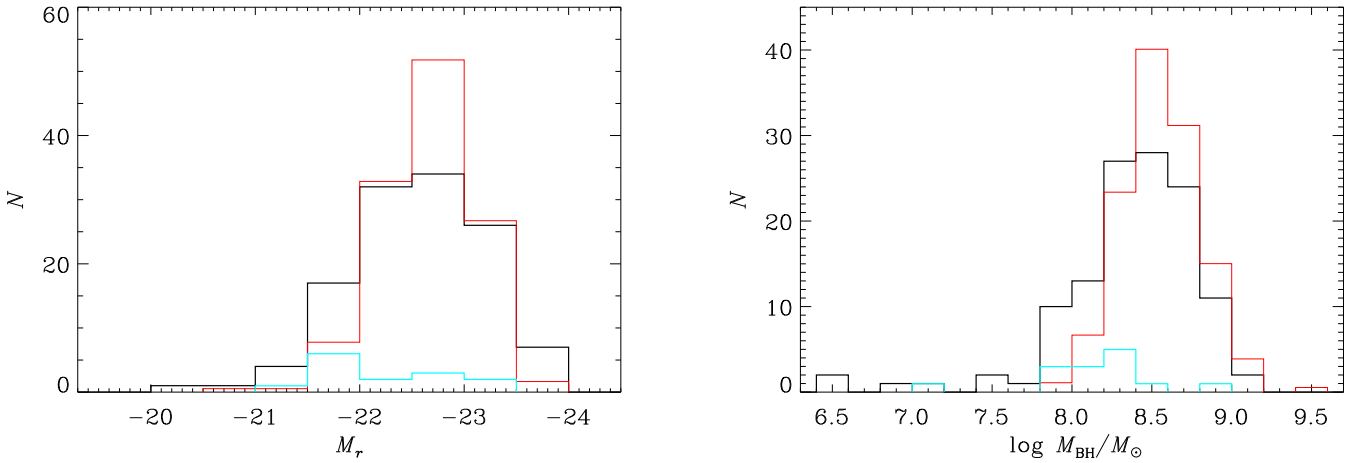

Fig. 1. Distributions of the *r*-band absolute magnitude (left) and black hole masses (right). The black histograms are for FRII*CAT* (cyan for the HEG FRII*CAT* subsample), the red histograms for the FRI*CAT*. The FRI*CAT* histograms are all scaled by the relative number of FR I and FR II, i.e., by 122/219.

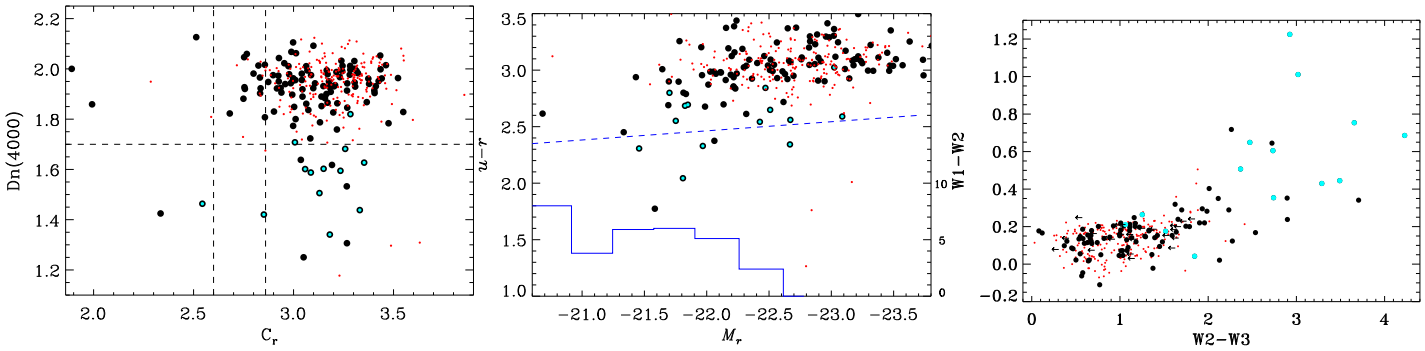

Fig. 2. Left: concentration index C_r vs. Dn(4000) index for the FRII*CAT* and FRI*CAT* samples indicated by black and red dots, respectively. The HEG FR II are represented by cyan circles. Center: absolute *r*-band magnitude, M_r, vs. $u - r$ color. Right: *WISE* mid-IR colors.

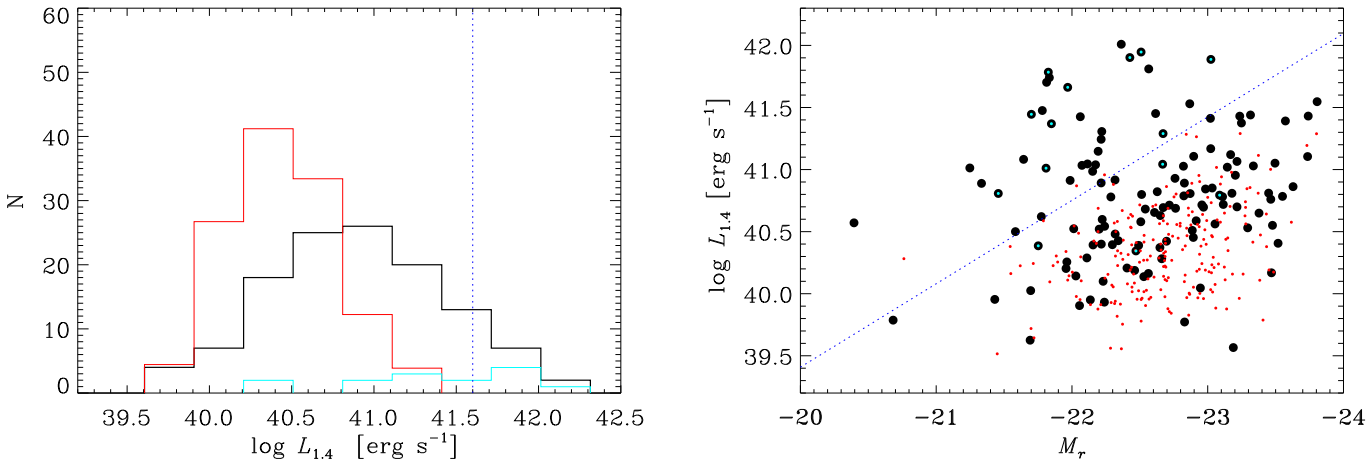

Fig. 3. Left panel: radio luminosity distribution of the FRII*CAT* (black, cyan for the HEGs) and FRI*CAT* sources (red). The dotted vertical line indicates the transition power between FR I and FR II reported by Fanaroff & Riley (1974). Right panel: radio luminosity (NVSS) vs. host absolute magnitude, M_r, for FRII*CAT* and FRI*CAT* (black and red, respectively; cyan for the HEG FR II). The dotted line shows the separation between FR I and FR II reported by Ledlow & Owen (1996) to which we applied a correction of 0.34 mag to account for the different magnitude definition and the color transformation between the SDSS and Cousin systems.

large black hole masses ($M_{\rm BH} \gtrsim 10^8 M_\odot$); only ~ 10% of the LEG FR IIs depart from this general description. All these properties are shared with the hosts of the FRI*CAT* sources. The distributions of $M_{\rm BH}$ and M_r differ with a statistical significance higher than 95% according to the Kolmogoroff-Smirnov test; this is due to the presence of a tail of low $M_{\rm BH}$ sources, reaching value as low as $3{\times}10^6 M_\odot$. However, the median of $M_{\rm BH}$ and M_r differ only marginally by less than 0.1 dex. Even the median radio luminosity of LEG FR II is just a factor ~3 higher than that measured in FR I. Apparently, the difference in radio morphology between edge-brightened and edge-darkened radio sources does not translate into a clear separation between the nuclear and host properties, while the spectroscopic classes, LEG and HEG, do.

The FRII*CAT* sample unveils a population of FR IIs of much lower radio power with respect to those obtained at high radio flux thresholds, extending it downward by two orders of magnitude. The correspondence of the morphological classification of FR I and FR II with a separation in radio power that is observed, for example, in the 3C sample, disappears. This conclusion is in line with previous results (Best 2009; Lin et al. 2010; Wing & Blanton 2011). A radio source produced by a low power jet can be edge brightened or edge darkened and the outcome is not due to differences in the optical properties of the host galaxy.

Nonetheless, Capetti et al. (2017) find that the connection between radio morphology and host properties is preserved in FR Is; there is a well-defined threshold of radio power above which an edge darkened radio source does not form and this limit has a strong positive dependence on the host luminosity. This effect was originally seen by Ledlow & Owen (1996) but partly lost in subsequent studies; we believe that we recover it because of the stricter criteria we adopted for the selection of FR Is.

It can be envisaged that brighter galaxies are associated with denser and more extended hot coronae that are able to disrupt more powerful jets. But the large population of low power FR IIs indicates that the situation is more complex; there is a large overlap of radio power between FR Is and FR IIs and radio power is believed to be a robust proxy for the jet power (e.g., Willott et al. 1999; Bîrzan et al. 2004). Apparently, jets of the same power expanding in similar galaxies can form both FR I and FR II. This indicates that the optical properties of the host and radio luminosity are not the only parameters driving the evolution of low power radio sources. Further studies of, for example, the X-rays properties and the larger scale environment are needed to clarify this issue.

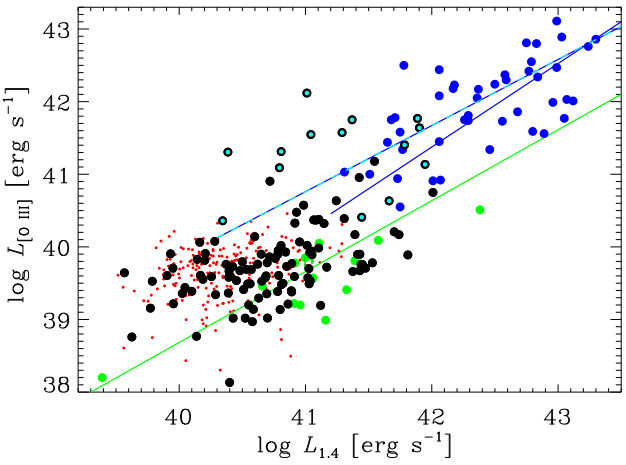

Fig. 4. Radio (NVSS) vs. [O III] line luminosity of the FRII*CAT* (black), FRI*CAT* (red), 3C-FR I (green), and 3C-FR II samples (blue) The green line (blue) shows the linear correlation between these two quantities derived from the FR Is (FR IIs) of the 3C sample from (Buttiglione et al. 2010). The dashed blue-cyan line is instead the linear fit on both the 3C and the FRII*CAT* HEGs.

References

Abazajian, K. N., Adelman-McCarthy, J. K., Agüeros, M. A., et al. 2009, ApJS, 182, 543
Baldi, R. D. & Capetti, A. 2008, A&A, 489, 989
Baldi, R. D. & Capetti, A. 2010, A&A, 519, A48+
Balogh, M. L., Morris, S. L., Yee, H. K. C., Carlberg, R. G., & Ellingson, E. 1999, ApJ, 527, 54
Becker, R. H., White, R. L., & Helfand, D. J. 1995, ApJ, 450, 559
Bell, E. F., McIntosh, D. H., Katz, N., & Weinberg, M. D. 2003, ApJS, 149, 289
Bernardi, M., Shankar, F., Hyde, J. B., et al. 2010, MNRAS, 404, 2087
Best, P. N. 2009, Astronomische Nachrichten, 330, 184
Best, P. N. & Heckman, T. M. 2012, MNRAS, 421, 1569
Bîrzan, L., Rafferty, D. A., McNamara, B. R., Wise, M. W., & Nulsen, P. E. J. 2004, ApJ, 607, 800
Brinchmann, J., Charlot, S., White, S. D. M., et al. 2004, MNRAS, 351, 1151
Buttiglione, S., Capetti, A., Celotti, A., et al. 2010, A&A, 509, A6
Capetti, A., Massaro, F., & Baldi, R. D. 2017, A&A, 598, A49
Capetti, A. & Raiteri, C. M. 2015, A&A, 580, A73
Condon, J. J., Cotton, W. D., Greisen, E. W., et al. 1998, AJ, 115, 1693
D'Abrusco, R., Massaro, F., Paggi, A., et al. 2013, ApJS, 206, 12
D'Abrusco, R., Massaro, F., Paggi, A., et al. 2014, ApJS, 215, 14
Fanaroff, B. L. & Riley, J. M. 1974, MNRAS, 167, 31P
Fukugita, M., Ichikawa, T., Gunn, J. E., et al. 1996, AJ, 111, 1748
Hardcastle, M. J., Evans, D. A., & Croston, J. H. 2007, MNRAS, 376, 1849
Helfand, D. J., White, R. L., & Becker, R. H. 2015, ApJ, 801, 26
Kauffmann, G., Heckman, T. M., White, S. D. M., et al. 2003, MNRAS, 341, 33
Kewley, L. J., Groves, B., Kauffmann, G., & Heckman, T. 2006, MNRAS, 372, 961
Laing, R. A., Jenkins, C. R., Wall, J. V., & Unger, S. W. 1994, in Astronomical Society of the Pacific Conference Series, Vol. 54, The Physics of Active Galaxies, ed. G. V. Bicknell, M. A. Dopita, & P. J. Quinn, 201
Ledlow, M. J. & Owen, F. N. 1996, AJ, 112, 9
Lin, Y.-T., Shen, Y., Strauss, M. A., Richards, G. T., & Lunnan, R. 2010, ApJ, 723, 1119
Miraghaei, H. & Best, P. N. 2017, MNRAS
Nakamura, O., Fukugita, M., Yasuda, N., et al. 2003, AJ, 125, 1682
Owen, F. N. & Rudnick, L. 1976, ApJ, 205, L1
Planck Collaboration, Ade, P. A. R., Aghanim, N., et al. 2016, A&A, 594, A13
Schawinski, K., Lintott, C., Thomas, D., et al. 2009, MNRAS, 396, 818
Shen, S., Mo, H. J., White, S. D. M., et al. 2003, MNRAS, 343, 978
Smolčić, V. 2009, ApJ, 699, L43
Stern, D., Eisenhardt, P., Gorjian, V., et al. 2005, ApJ, 631, 163
Strateva, I., Ivezić, Ž., Knapp, G. R., et al. 2001, AJ, 122, 1861
Tremaine, S., Gebhardt, K., Bender, R., et al. 2002, ApJ, 574, 740
Tremonti, C. A., Heckman, T. M., Kauffmann, G., et al. 2004, ApJ, 613, 898
Willott, C. J., Rawlings, S., Blundell, K. M., & Lacy, M. 1999, MNRAS, 309, 1017
Wing, J. D. & Blanton, E. L. 2011, AJ, 141, 88
Wright, E. L., Eisenhardt, P. R. M., Mainzer, A. K., et al. 2010, AJ, 140, 1868

Acknowledgements. F.M. gratefully acknowledges the financial support of the Programma Giovani Ricercatori – Rita Levi Montalcini – Rientro dei Cervelli (2012) awarded by the Italian Ministry of Education, Universities and Research (MIUR).

Part of this work is based on the NVSS (NRAO VLA Sky Survey): The National Radio Astronomy Observatory is operated by Associated Universities, Inc., under contract with the National Science Foundation.

This publication makes use of data products from the Wide-field Infrared Survey Explorer, which is a joint project of the University of California, Los Angeles, and the Jet Propulsion Laboratory/California Institute of Technology, funded by the National Aeronautics and Space Administration.

This research made use of the NASA/ IPAC Infrared Science Archive and Extragalactic Database (NED), which are operated by the Jet Propulsion Laboratory, California Institute of Technology, under contract with the National Aeronautics and Space Administration.

We acknowledge the usage of the HyperLeda database (http://leda.univ-lyon1.fr).

Funding for SDSS-III has been provided by the Alfred P. Sloan Foundation, the Participating Institutions, the National Science Foundation, and the U.S. Department of Energy Office of Science. The SDSS-III website is http://www.sdss3.org/. SDSS-III is managed by the Astrophysical Research Consortium for the Participating Institutions of the SDSS-III Collaboration, including the University of Arizona, the Brazilian Participation Group, Brookhaven National Laboratory, University of Cambridge, Carnegie Mellon University, University of Florida, the French Participation Group, the German Participation Group, Harvard University, the Instituto de Astrofisica de Canarias, the Michigan State/Notre Dame/JINA Participation Group, Johns Hopkins University, Lawrence Berkeley National Laboratory, Max Planck Institute for Astrophysics, Max Planck Institute for Extraterrestrial Physics, New Mexico State University, New York University, Ohio State University, Pennsylvania State University, University of Portsmouth, Princeton University, the Spanish Participation Group, University of Tokyo, University of Utah, Vanderbilt University, University of Virginia, University of Washington, and Yale University.

Table 1. Properties of the FRII*CAT* sources.

	z	NVSS	[O III]	m_r	Dn	σ_*	C_r	νL_r	$L_{[O\ III]}$	M_{BH}	Class
SDSS J001247.57+004715.8	0.148	58.6	11.5	16.352	2.07	263	2.99	40.72	39.86	8.6	LEG
SDSS J002107.62−005531.4	0.108	111.9	3.3	15.351	1.99	250	3.17	40.70	39.02	8.5	LEG
SDSS J004326.80−105421.8	0.127	82.3	176.6	15.834	1.92	247	2.92	40.72	40.90	8.5	LEG
SDSS J004404.66+010152.9	0.112	366.0	126.1	16.426	1.78	219	3.48	41.24	40.64	8.3	LEG
SDSS J011830.65−104356.4	0.126	56.3	7.0	16.681	1.83	224	2.90	40.54	39.49	8.3	LEG
SDSS J024558.54−064900.6	0.139	102.0	4.4	16.318	1.86	261	3.06	40.89	39.38	8.6	LEG
SDSS J075221.83+333348.9	0.140	66.0	—	16.458	1.95	269	3.31	40.71	—	8.6	LEG
SDSS J075529.95+520450.6	0.140	99.4	4.5	17.835	1.42	81	2.33	40.89	39.39	6.6	LEG
SDSS J075628.78+501716.3	0.134	165.0	46.8	15.844	1.93	296	2.75	41.07	40.37	8.8	LEG
SDSS J080107.19+175849.7	0.140	847.0	9.7	17.417	1.57	161	2.85	41.82	39.73	7.7	LEG
SDSS J080158.09+175152.6	0.147	16.9	18.8	16.715	1.99	258	3.24	40.16	40.06	8.6	LEG
SDSS J080535.00+240950.3	0.060	4781.0	2791.1	15.376	1.68	205	3.26	41.78	41.40	8.2	HEG
SDSS J081343.61+525738.2	0.138	194.6	9.7	16.116	1.98	250	2.80	41.17	39.72	8.5	LEG
SDSS J081512.33+384045.4	0.125	487.8	11.6	17.127	1.88	333	2.75	41.48	39.71	9.0	LEG
SDSS J081734.46+445850.8	0.142	135.6	6.0	17.032	1.98	234	3.28	41.04	39.54	8.4	LEG
SDSS J082247.63+041750.0	0.095	132.0	13.7	15.666	1.94	248	3.27	40.65	39.53	8.5	LEG
SDSS J083109.54+414738.1	0.132	155.0	10.2	16.211	2.01	236	3.28	41.03	39.70	8.4	LEG
SDSS J083112.15+434158.4	0.111	121.0	20.4	15.170	1.84	275	3.07	40.76	39.84	8.7	LEG
SDSS J084529.04+421952.9	0.133	201.0	42.0	16.857	1.79	230	3.13	41.15	40.32	8.4	LEG
SDSS J084759.04+314708.3	0.067	1647.0	67.7	13.735	2.02	338	2.95	41.43	39.90	9.0	LEG
SDSS J090150.32+555527.4	0.141	638.0	28.5	17.372	1.85	191	3.00	41.70	40.21	8.1	LEG
SDSS J091153.61+372413.3	0.104	596.4	50.0	14.908	1.95	301	2.87	41.39	40.17	8.8	LEG
SDSS J091225.08+534139.1	0.101	204.1	21.6	16.181	1.77	183	3.00	40.89	39.77	8.0	LEG
SDSS J091445.53+413714.2	0.140	449.0	269.1	15.371	1.82	300	2.68	41.55	41.18	8.8	LEG
SDSS J091948.45+575055.9	0.137	11.5	15.1	16.879	1.94	261	3.21	39.93	39.90	8.6	LEG
SDSS J092611.26+170357.9	0.116	163.3	80.6	15.972	1.93	233	3.44	40.93	40.48	8.4	LEG
SDSS J093215.91+180419.9	0.147	57.0	9.7	16.324	2.00	271	3.41	40.70	39.78	8.7	LEG
SDSS J093641.99+111350.9	0.120	48.3	2.6	16.457	1.96	298	3.44	40.43	39.02	8.8	LEG
SDSS J094124.02+394441.8	0.108	1811.0	1382.7	16.125	1.60	209	3.06	41.90	41.64	8.2	HEG
SDSS J094201.76+084736.8	0.134	97.6	16.6	16.092	1.93	292	3.15	40.84	39.93	8.8	LEG
SDSS J094703.01+231614.2	0.084	30.8	21.7	15.923	1.93	234	3.18	39.90	39.61	8.4	LEG
SDSS J095640.77−000124.0	0.139	166.0	43.4	16.259	2.04	265	2.93	41.11	40.38	8.6	LEG
SDSS J101558.24+404647.2	0.128	1009.0	16.9	16.392	1.91	236	3.40	41.81	39.89	8.4	LEG
SDSS J101954.48+393022.8	0.112	52.0	0.4	16.433	1.86	227	3.22	40.40	38.13	8.4	LEG
SDSS J102150.38+080833.8	0.103	585.7	15.8	15.211	1.90	253	2.99	41.38	39.66	8.5	LEG
SDSS J102156.67+144331.4	0.111	412.0	1110.3	15.956	1.60	193	3.05	41.29	41.57	8.1	HEG
SDSS J102237.40+383444.9	0.052	117.4	40.8	13.935	1.96	268	3.01	40.05	39.44	8.6	LEG
SDSS J103128.22+084324.1	0.141	347.7	10.2	15.871	1.97	229	2.92	41.44	39.76	8.4	LEG
SDSS J103443.26+053319.8	0.141	167.1	2.8	16.015	2.03	279	3.30	41.12	39.19	8.7	LEG
SDSS J103602.94+525936.1	0.142	30.1	350.0	17.456	1.59	170	3.09	40.39	41.31	7.8	HEG
SDSS J104502.74+471759.1	0.145	76.2	17.4	16.381	1.98	289	3.32	40.81	40.02	8.8	LEG
SDSS J104632.21+543559.7	0.145	279.0	938.6	17.400	1.44	302	3.33	41.37	41.75	8.8	HEG
SDSS J104742.83+434652.7	0.086	104.0	17.6	15.137	2.01	230	2.97	40.45	39.54	8.4	LEG
SDSS J105052.47+400050.7	0.129	147.0	79.7	16.833	1.83	204	3.20	40.99	40.57	8.2	LEG
SDSS J105439.55+060630.7	0.135	58.7	3.8	16.442	1.94	226	3.38	40.63	39.29	8.3	LEG
SDSS J110035.08+253911.0	0.145	242.0	41.0	17.027	1.95	228	3.20	41.31	40.39	8.4	LEG
SDSS J110151.89+164038.6	0.069	699.0	188.9	15.891	1.93	226	3.23	41.08	40.37	8.3	LEG
SDSS J110214.15+242954.7	0.144	108.0	19.7	16.038	1.94	282	3.31	40.95	40.07	8.7	LEG
SDSS J110214.91+234111.9	0.146	29.0	6.3	17.111	1.90	184	3.11	40.39	39.58	8.0	LEG
SDSS J110215.68+290725.2	0.106	145.6	402.7	15.429	1.51	219	3.08	40.79	41.09	8.3	HEG
SDSS J110253.95+125904.0	0.140	82.0	16.6	15.999	1.96	253	3.04	40.81	39.97	8.5	LEG
SDSS J111317.91+412429.3	0.095	115.2	5.8	15.340	1.94	202	2.99	40.59	39.14	8.1	LEG
SDSS J112126.44+534456.7	0.104	83.0	16.8	15.175	1.90	215	2.83	40.53	39.69	8.3	LEG
SDSS J113133.57+604727.9	0.145	19.0	10.9	17.294	1.91	190	2.94	40.20	39.81	8.0	LEG
SDSS J113626.35+501323.7	0.054	41.0	7.8	15.280	1.91	173	3.19	39.63	38.76	7.9	LEG
SDSS J114427.19+370831.8	0.115	2012.0	154.7	16.341	1.87	225	3.52	42.01	40.75	8.3	LEG
SDSS J114428.11+035815.7	0.127	75.6	8.3	16.408	1.85	248	3.14	40.68	39.57	8.5	LEG
SDSS J114432.99+213217.0	0.109	35.3	24.8	16.183	1.97	263	3.21	40.21	39.91	8.6	LEG
SDSS J114525.98−022332.9	0.128	46.8	10.2	16.648	1.92	248	2.94	40.48	39.67	8.5	LEG
SDSS J114948.11+435412.6	0.071	58.0	17.5	15.898	1.96	229	3.37	40.02	39.36	8.4	LEG

Continued on Next Page

Table 1 – Continued

	z	NVSS	[O III]	m_r	Dn	σ_*	C_r	νL_r	$L_{[O\ III]}$	M_{BH}	Class
SDSS J115358.87+093929.8	0.103	672.0	16.4	15.211	1.99	267	3.07	41.43	39.67	8.6	LEG
SDSS J115525.19+253222.4	0.137	26.1	4.1	17.009	1.99	263	3.15	40.29	39.34	8.6	LEG
SDSS J115812.96+300625.9	0.139	106.7	7.1	17.165	1.72	96	1.99	40.91	39.59	6.8	LEG
SDSS J115820.13+262112.0	0.112	1142.0	42.8	16.813	1.86	198	3.18	41.74	40.17	8.1	LEG
SDSS J120732.92+335240.1	0.079	480.7	2148.6	15.175	1.34	192	2.75	41.04	41.55	8.1	HEG
SDSS J122052.45+313308.4	0.104	60.3	15.8	16.179	1.96	241	3.18	40.39	39.67	8.5	LEG
SDSS J122640.22+253855.5	0.134	44.3	12.2	17.490	1.25	76	1.89	40.50	39.80	6.5	LEG
SDSS J124021.98+465636.3	0.141	135.5	14.5	17.121	1.85	175	3.27	41.03	39.92	7.9	LEG
SDSS J125222.61+031554.0	0.099	919.0	22.9	15.489	1.98	246	3.04	41.53	39.78	8.5	LEG
SDSS J125303.17+450044.8	0.078	472.0	23.7	14.659	1.97	253	2.90	41.02	39.57	8.5	LEG
SDSS J131509.84+084053.3	0.093	869.0	111.7	16.504	1.82	219	3.28	41.45	40.41	8.3	HEG
SDSS J131904.16+293834.8	0.073	1467.0	41.5	15.036	1.87	202	3.17	41.45	39.76	8.2	LEG
SDSS J132117.81+423515.2	0.079	1985.0	259.8	15.883	1.46	176	2.54	41.66	40.63	7.9	HEG
SDSS J132848.45+275227.8	0.091	207.0	927.0	16.711	1.42	177	3.37	40.81	41.31	7.9	HEG
SDSS J133453.36−013238.5	0.087	22.0	16.9	17.369	1.81	132	2.86	39.79	39.53	7.4	LEG
SDSS J133729.21+481820.5	0.119	69.0	2.4	16.285	1.89	234	3.04	40.58	38.97	8.4	LEG
SDSS J133742.35+294223.2	0.115	219.0	21.2	15.222	2.05	269	3.01	41.05	39.89	8.6	LEG
SDSS J134134.85+534443.7	0.141	1118.0	241.9	16.677	1.59	240	3.23	41.95	41.14	8.4	HEG
SDSS J134503.02+094724.0	0.130	73.0	8.3	16.239	1.92	242	3.04	40.69	39.60	8.5	LEG
SDSS J134532.76+054610.4	0.125	81.0	5.2	16.231	1.93	239	3.41	40.69	39.35	8.4	LEG
SDSS J135117.87+640936.9	0.109	39.3	11.9	16.632	1.89	165	3.14	40.26	39.59	7.8	LEG
SDSS J135124.55+085216.4	0.136	88.0	5.8	15.656	2.01	298	3.06	40.81	39.48	8.8	LEG
SDSS J135432.96+281436.1	0.065	84.0	22.8	15.150	2.06	221	3.28	40.10	39.39	8.3	LEG
SDSS J135526.20+352544.1	0.108	53.0	18.1	15.911	1.91	205	3.27	40.37	39.76	8.2	LEG
SDSS J141231.76+140041.0	0.140	46.9	5.6	16.113	2.01	305	3.24	40.56	39.49	8.9	LEG
SDSS J141247.44+045431.5	0.136	36.3	10.3	16.401	1.90	233	3.16	40.42	39.73	8.4	LEG
SDSS J141527.22+172431.1	0.124	9.8	3.3	16.063	2.00	313	3.46	39.77	39.16	8.9	LEG
SDSS J142341.44+250149.2	0.146	28.8	3.8	16.773	2.00	263	3.00	40.39	39.36	8.6	LEG
SDSS J142557.05+392444.9	0.143	27.0	39.1	16.752	1.71	220	3.01	40.34	40.36	8.3	HEG
SDSS J143010.53+304428.3	0.129	49.4	5.5	16.095	1.95	211	2.96	40.51	39.41	8.2	LEG
SDSS J143715.00+244532.2	0.086	151.6	29.4	16.267	1.94	210	3.35	40.62	39.76	8.2	LEG
SDSS J144625.13+214209.8	0.112	7.6	12.7	15.465	1.98	264	3.31	39.57	39.64	8.6	
SDSS J144626.18+063359.1	0.063	64.1	16.4	15.877	1.95	168	2.93	39.95	39.22	7.8	LEG
SDSS J144948.90+335126.8	0.088	116.0	5.1	16.074	1.83	223	3.55	40.52	39.02	8.3	LEG
SDSS J145423.45+162119.0	0.045	1489.0	60.5	13.245	2.01	304	3.09	41.03	39.49	8.9	LEG
SDSS J145752.76+111809.5	0.122	105.2	9.7	16.031	2.03	247	3.24	40.79	39.61	8.5	LEG
SDSS J145753.81+283218.7	0.144	930.0	990.4	16.214	1.63	232	2.84	41.89	41.77	8.4	HEG
SDSS J150031.48+362849.8	0.093	59.7	52.1	15.543	1.92	260	3.10	40.28	40.08	8.6	LEG
SDSS J150146.57+243916.0	0.120	108.3	22.2	15.263	1.92	261	2.77	40.78	39.95	8.6	LEG
SDSS J150827.31+541507.4	0.096	25.7	20.5	16.156	1.62	187	3.19	39.95	39.71	8.0	LEG
SDSS J151247.16−014423.3	0.146	120.0	2148.5	17.461	1.04	110	2.54	41.01	42.12	7.1	HEG
SDSS J151414.68+232708.4	0.088	232.7	15.4	15.449	2.06	238	3.27	40.82	39.50	8.4	LEG
SDSS J151423.26+011130.7	0.125	54.0	—	16.709	1.97	189	2.83	40.52	—	8.0	LEG
SDSS J151454.07+420047.3	0.135	177.0	18.8	15.346	1.98	315	3.17	41.10	39.99	8.9	LEG
SDSS J151639.48+024712.6	0.110	131.0	24.1	15.491	1.88	273	3.16	40.78	39.90	8.7	LEG
SDSS J151640.21+001501.9	0.053	2722.0	1286.6	14.855	1.31	293	3.27	41.43	40.95	8.8	LEG
SDSS J152245.61+194220.3	0.109	86.7	42.3	16.368	1.53	209	3.10	40.60	40.14	8.2	LEG
SDSS J152257.38+025512.1	0.110	29.4	1.8	16.084	2.13	213	2.51	40.14	38.77	8.2	LEG
SDSS J153007.96+231616.0	0.090	236.0	25.0	15.103	2.09	287	3.00	40.85	39.73	8.8	LEG
SDSS J154042.39+422136.0	0.142	55.3	13.8	15.829	2.01	279	2.82	40.65	39.90	8.7	LEG
SDSS J154118.78+514043.6	0.148	40.3	2.5	15.827	2.11	260	3.00	40.55	39.20	8.6	LEG
SDSS J155700.17+413111.1	0.085	140.0	25.7	17.607	1.76	139	3.22	40.57	39.69	7.5	LEG
SDSS J155852.66+262618.9	0.087	52.0	20.0	14.601	1.98	282	2.98	40.17	39.61	8.7	LEG
SDSS J160909.44+162549.9	0.143	88.7	2.8	15.598	1.96	297	3.13	40.86	39.21	8.8	LEG
SDSS J161057.11+032202.8	0.119	109.1	6.2	16.508	2.00	229	3.31	40.78	39.39	8.4	LEG
SDSS J162046.64+430911.4	0.134	35.9	7.7	15.550	2.02	293	2.86	40.41	39.59	8.8	LEG
SDSS J163604.21+271829.0	0.134	363.0	15.4	16.051	1.99	263	3.01	41.41	39.89	8.6	LEG
SDSS J164857.35+260441.1	0.137	137.7	19.6	17.877	1.94	178	3.18	41.01	40.02	7.9	LEG
SDSS J164924.01+263502.6	0.055	146.0	47.4	14.537	1.92	223	2.76	40.19	39.55	8.3	LEG
SDSS J165847.14+625624.6	0.106	258.0	28.4	16.410	1.80	175	3.01	41.05	39.94	7.9	LEG
SDSS J214801.27−082527.5	0.135	88.0	2.7	16.564	2.05	189	3.43	40.80	39.14	8.0	LEG

Continued on Next Page

Table 1 – Continued

	z	NVSS	[O III]	m_r	Dn	σ_*	C_r	νL_r	$L_{[\mathrm{O\ III}]}$	M_{BH}	Class
SDSS J231542.10−002607.0	0.091	45.0	30.5	16.136	1.95	280	3.43	40.14	39.83	8.7	LEG
SDSS J232710.69−004157.8	0.099	223.0	80.4	16.043	1.64	223	3.04	40.92	40.33	8.3	LEG

Column description: (1) source name; (2) redshift; (3) NVSS 1.4 GHz flux density [mJy]; (4) [O III] flux [in 10^{-17} erg cm^{-2} s^{-1} units]; (5) SDSS DR7 r band AB magnitude; (6) concentration index C_r; (7) Dn(4000) index; (8) stellar velocity dispersion [km s^{-1}]; (9) logarithm of the radio luminosity [erg s^{-1}]; (10) logarithm of the [O III] line luminosity [erg s^{-1}]; (11) logarithm of the black hole mass [in solar units]; (12) spectroscopic class.

Appendix A: FIRST images of the FRII*CAT* sources.

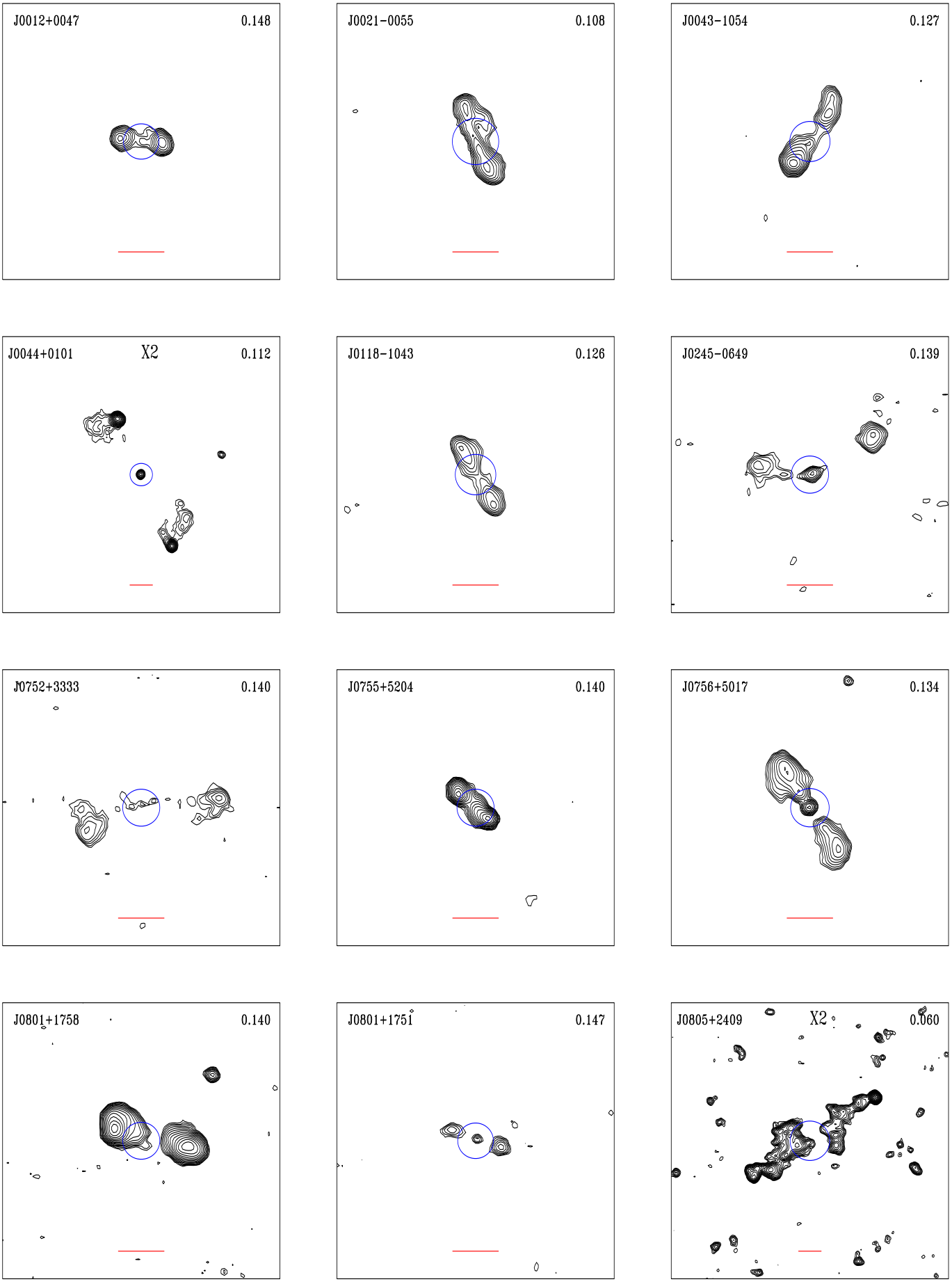

Fig. A.1. Images of the FR IIs selected. Contours are drawn starting from 0.45 mJy/beam and increase with a geometric progression with a common ratio of $\sqrt{2}$. The field of view is 3'×3' in most cases, except for those marked with a 'X2' at the top; the red tick at the bottom is 30″ long. The blue circle is centered on the host galaxy and has a radius of 30 kpc. The source ID and redshift are reported in the upper corners.

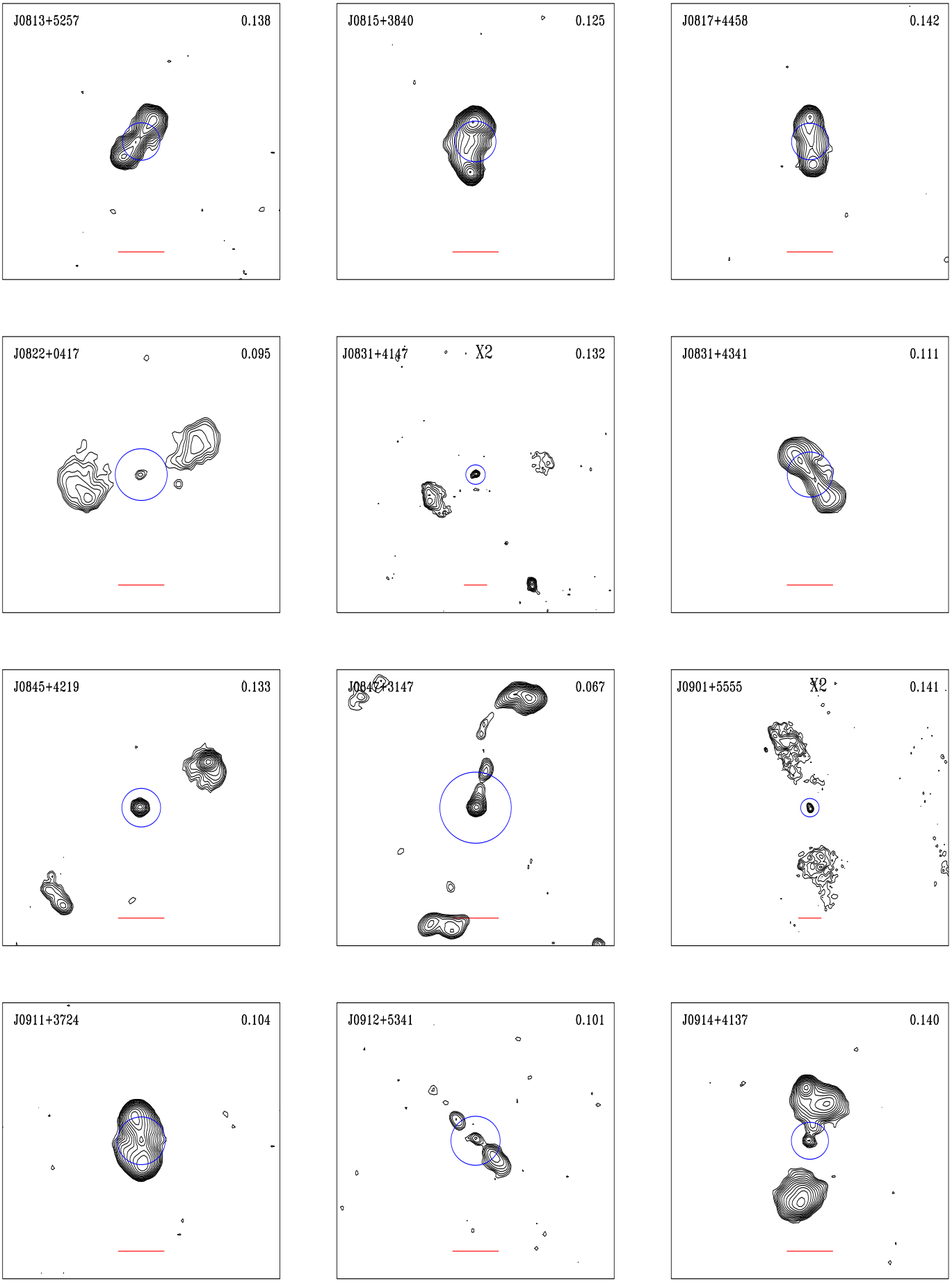

Fig. A.2. (continued)

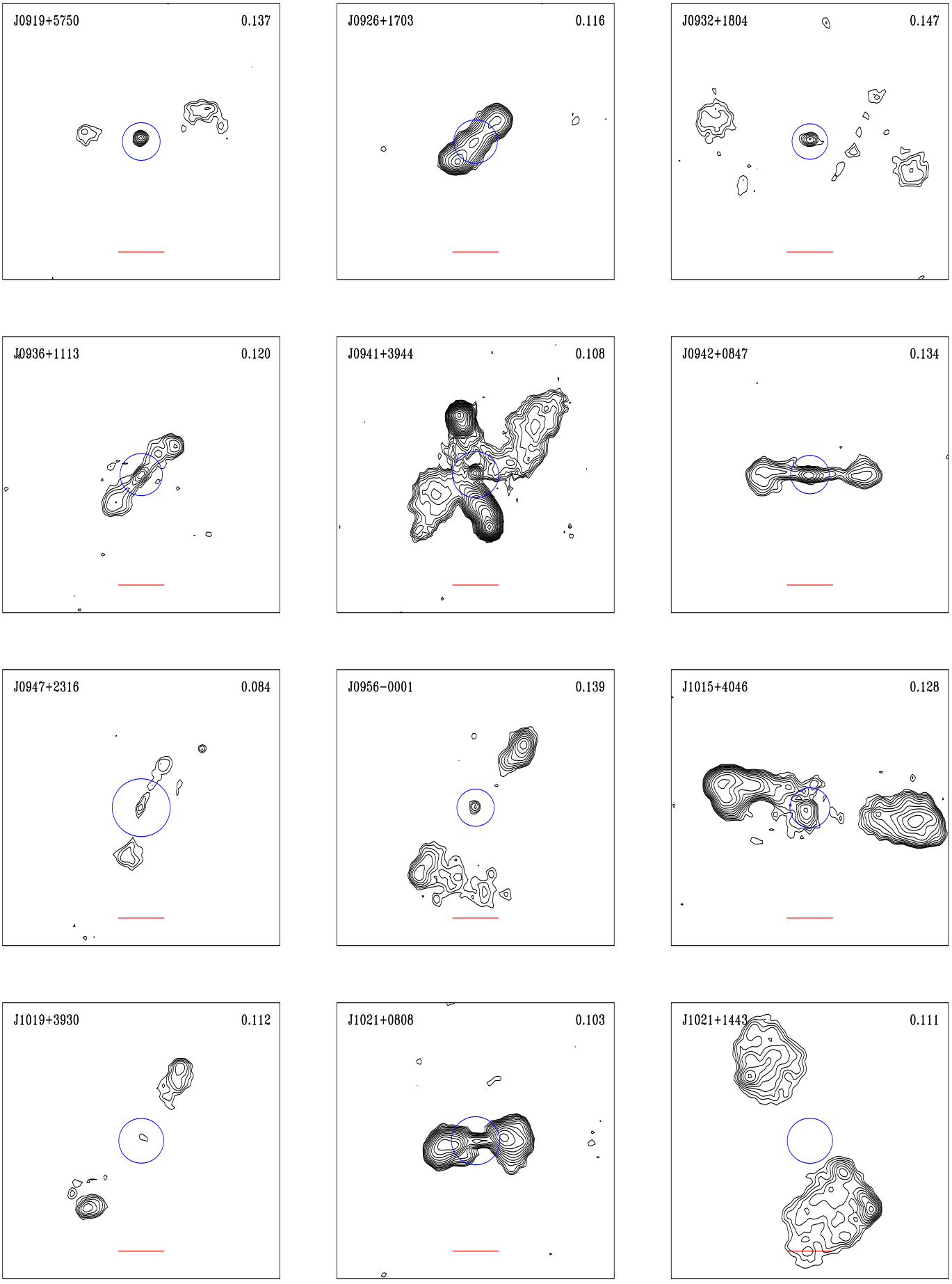

Fig. A.2. (continued)

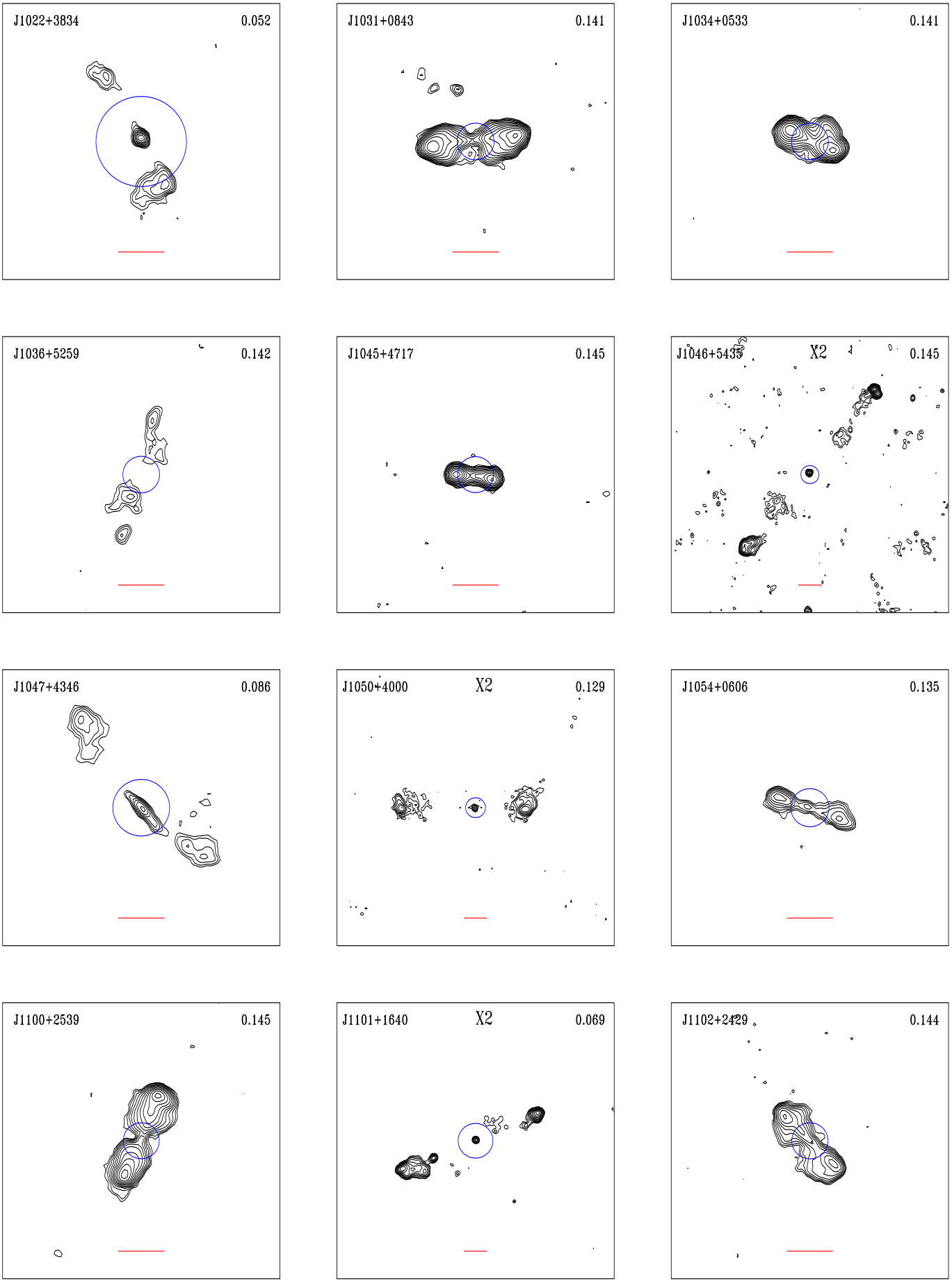

Fig. A.2. (continued)

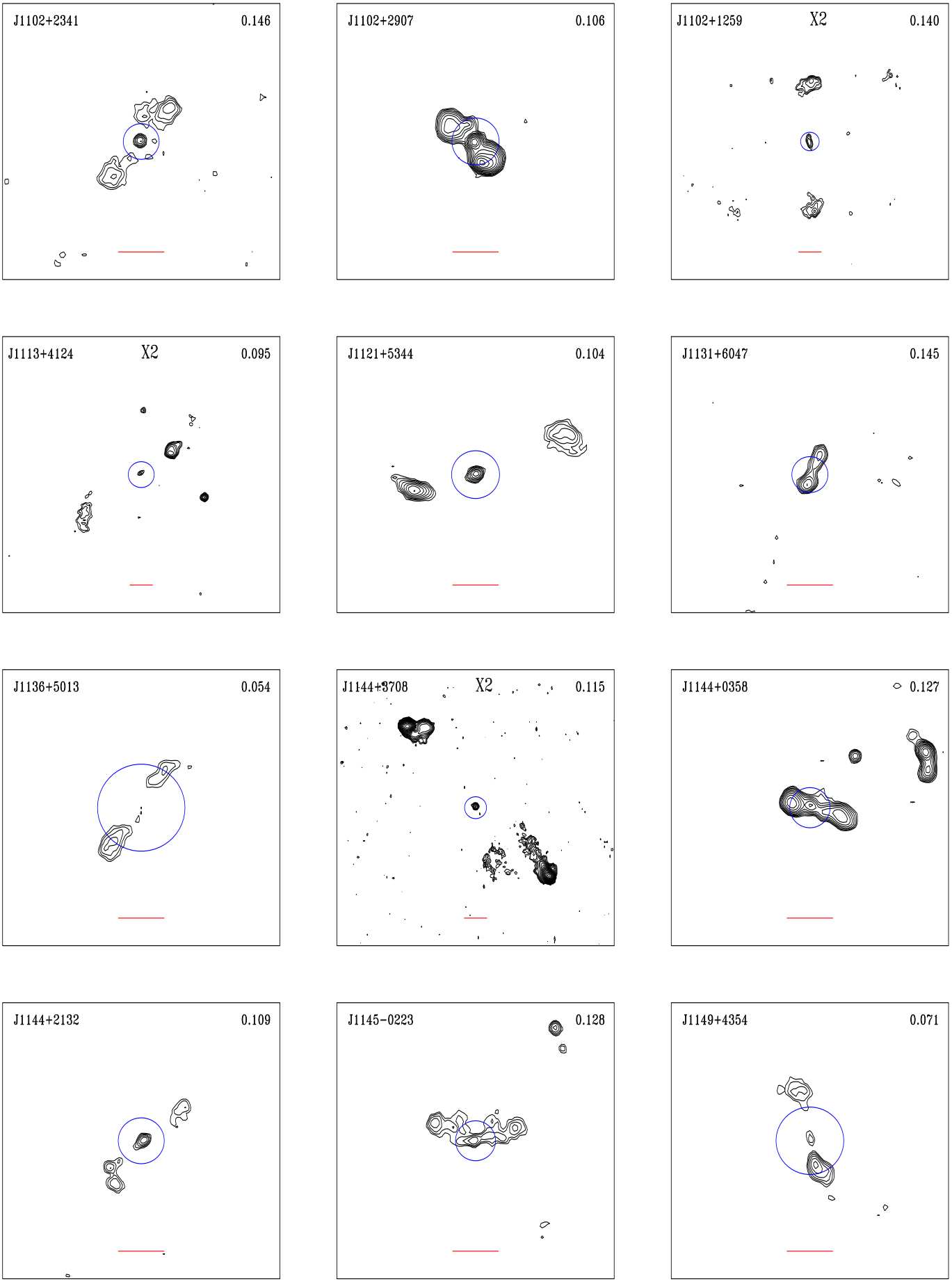

Fig. A.2. (continued)

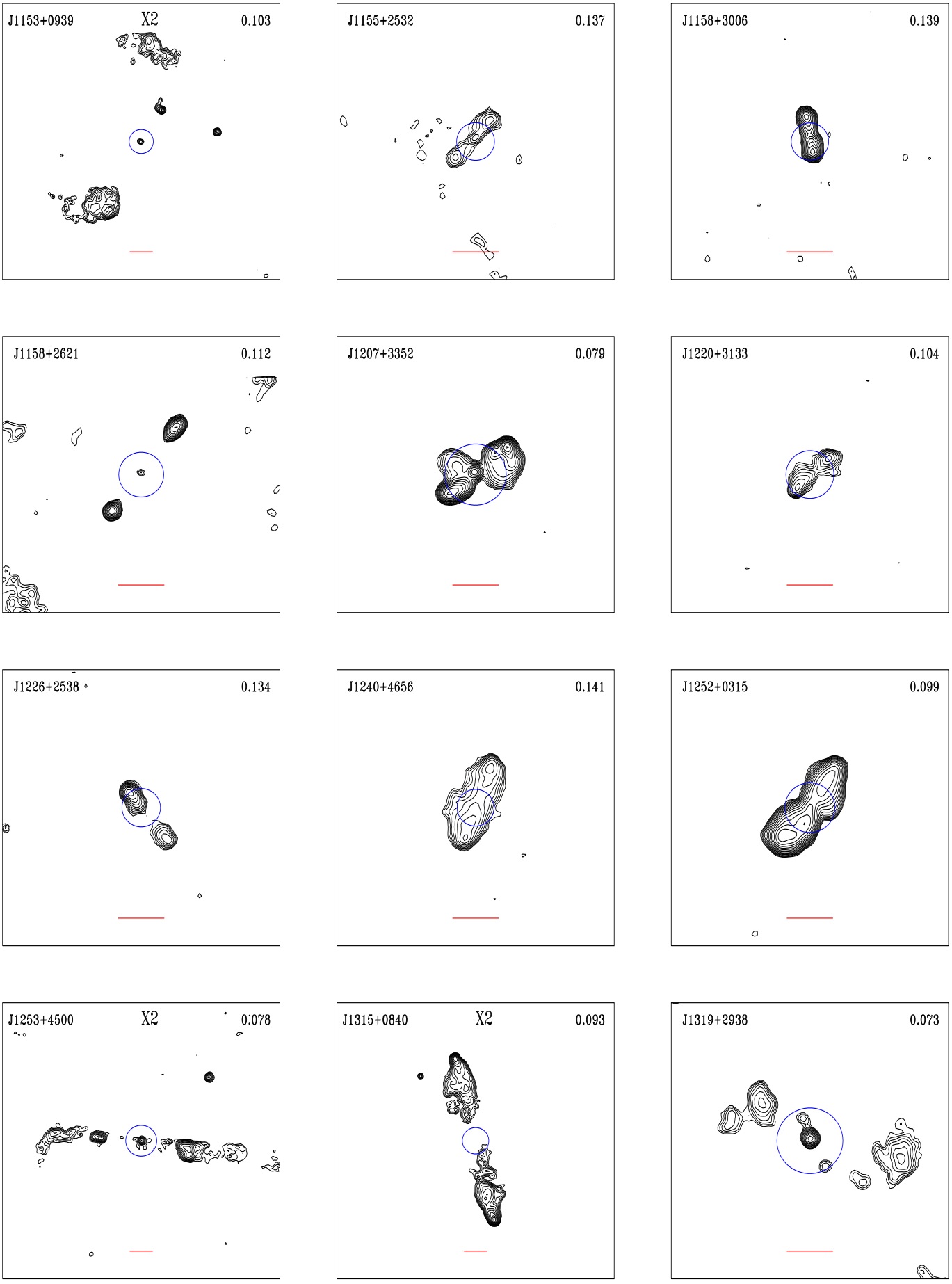

Fig. A.2. (continued)

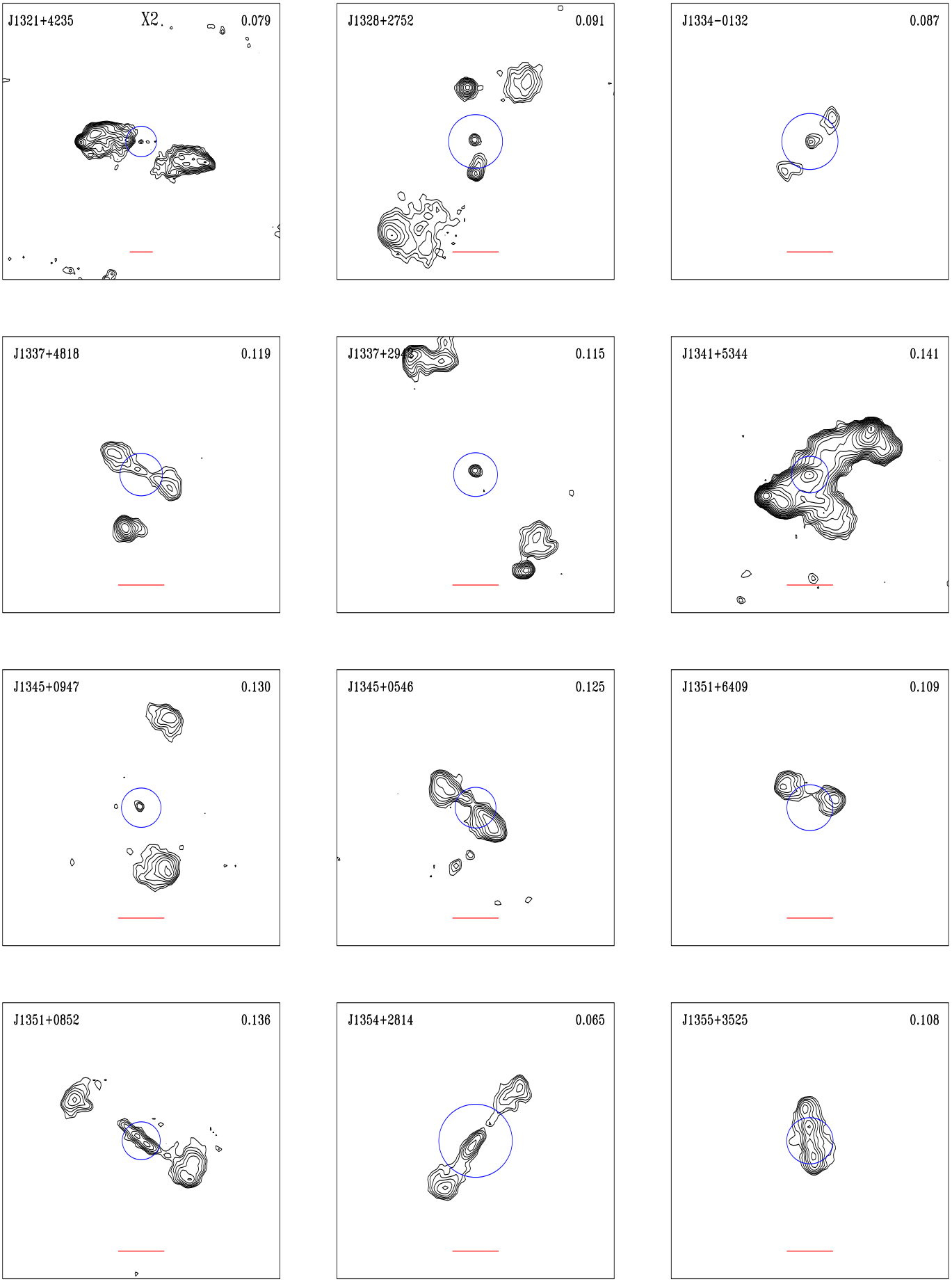

Fig. A.2. (continued)

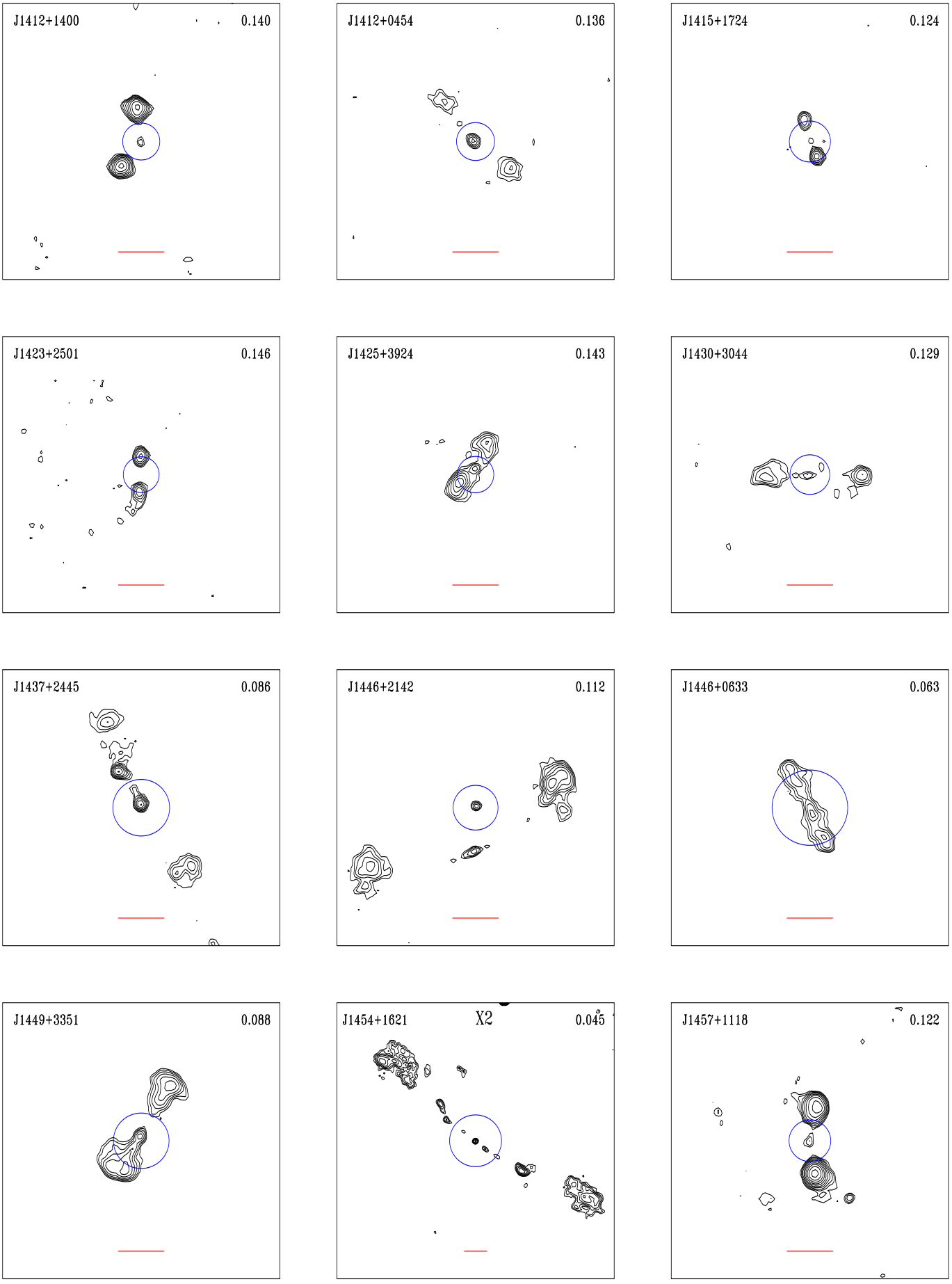

Fig. A.2. (continued)

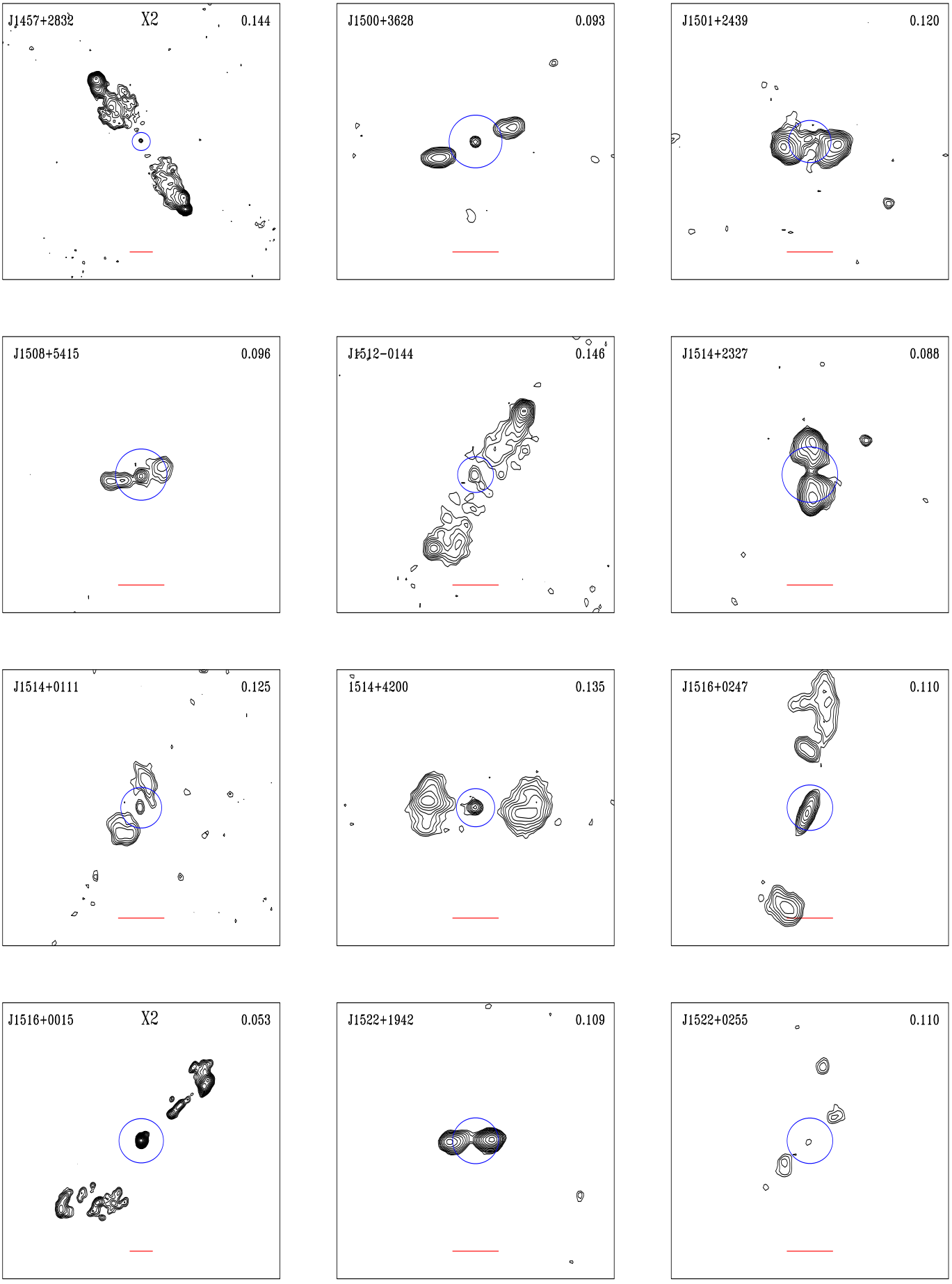

Fig. A.2. (continued)

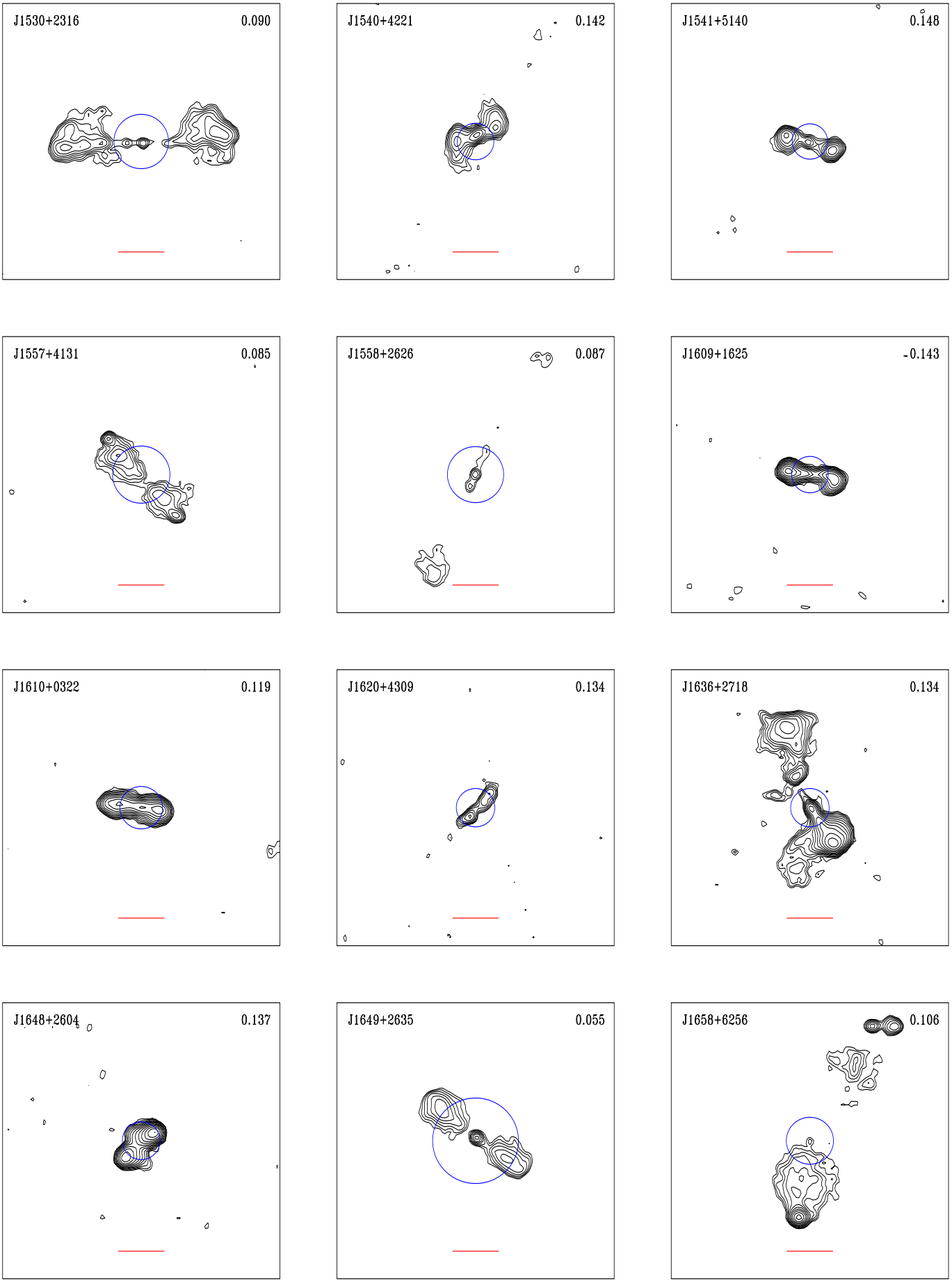

Fig. A.2. (continued)

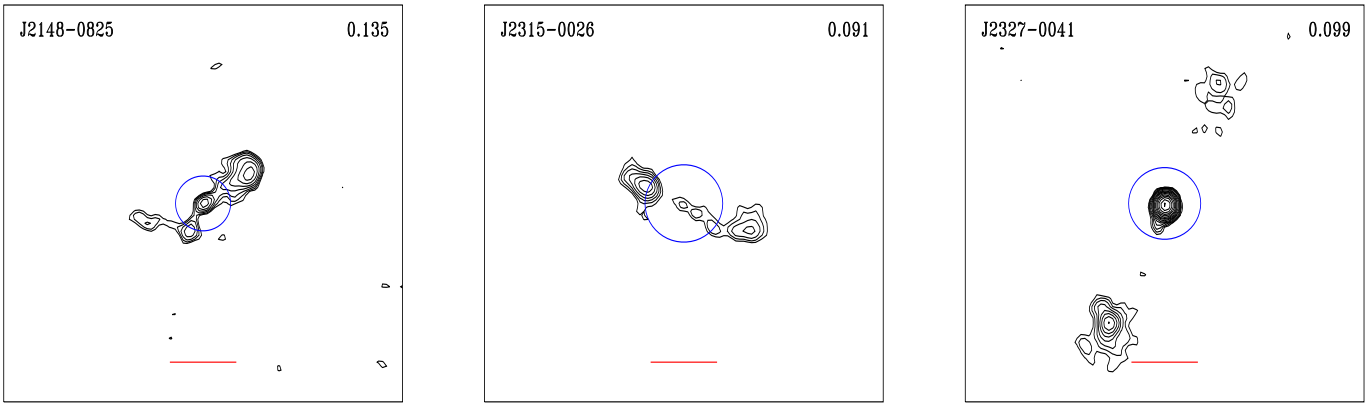

Fig. A.2. (continued)